314–326 *Nucleic Acids Research, 2010, Vol. 38, No. 1* *Published online 23 October 2009*
doi:10.1093/nar/gkp736

Fine tuning of the *E. coli* NusB:NusE complex affinity to *BoxA* RNA is required for processive antitermination

Björn M. Burmann[1], Xiao Luo[2,3], Paul Rösch[1,*], Markus C. Wahl[2,3] and Max E. Gottesman[4]

[1]Lehrstuhl Biopolymere und Forschungszentrum für Bio-Makromoleküle, Universität Bayreuth, Universitätsstraße 30, 95447 Bayreuth, [2]Max-Planck-Institut für biophysikalische Chemie, Makromolekulare Röntgenkristallographie, Am Faßberg 11, 37077 Göttingen, [3]Freie Universität Berlin, Fachbereich Biologie-Chemie-Pharmazie, Institut für Chemie und Biochemie, AG Strukturbiochemie, Takustr. 6, 14195 Berlin, Germany and [4]Department of Microbiology and Institute of Cancer Research, Columbia University Medical Center, New York, NY 10032, USA

Received July 22, 2009; Revised and Accepted August 20, 2009

ABSTRACT

Phage λ propagation in *Escherichia coli* host cells requires transcription antitermination on the λ chromosome mediated by λN protein and four host Nus factors, NusA, B, E (ribosomal S10) and G. Interaction of *E. coli* NusB:NusE heterodimer with the single stranded *BoxA* motif of λ*nutL* or λ*nutR* RNA is crucial for this reaction. Similarly, binding of NusB:NusE to a *BoxA* motif is essential to suppress transcription termination in the ribosomal RNA (*rrn*) operons. We used fluorescence anisotropy to measure the binding properties of NusB and of NusB:NusE heterodimer to *BoxA*-containing RNAs differing in length and sequence. Our results demonstrate that *BoxA* is necessary and sufficient for binding. We also studied the gain-of-function D118N NusB mutant that allows λ growth in *nusA1* or *nusE71* mutants. *In vivo* λ burst-size determinations, CD thermal unfolding measurements and X-ray crystallography of this as well as various other NusB D118 mutants showed the importance of size and polarity of amino acid 118 for RNA binding and other interactions. Our work suggests that the affinity of the NusB:NusE complex to *BoxA* RNA is precisely tuned to maximize control of transcription termination.

INTRODUCTION

Phage λ-mediated antitermination in *Escherichia coli* enables RNA polymerase (RNAP) to read through early transcription termination sites on the phage chromosome (1). Antitermination is regulated *via* the direct interaction of N protein and the transcription elongation complex (TEC) formed by RNA, RNAP and the Nus (N utilization substance) host factors NusA, NusB, NusE (S10 ribosomal protein) and NusG (2–4). N-mediated antitermination is coupled to transcription of the phage λ *nut* RNA sites, each consisting of the single stranded *BoxA* and the palindromic stem–loop *BoxB* linked by a *spacer* sequence to which NusA binds (5). N interacts with *BoxB* and converts the TEC to a termination-resistant form (6,7). Binding of λ N to *BoxB* results in an indirect interaction with RNAP through NusA (8,9). NusB interacts with the *nut* site by binding to *BoxA*, an interaction that is ∼10-fold strengthened upon NusE:NusB heterodimer formation (10–13). The NusB:NusE:RNA ternary complex is proposed to associate with RNAP through NusE (1,14,15). A similar complex in which λ N is replaced by phage HK022 Nun protein induces transcription arrest on the λ chromosome (7).

In addition to its involvement in transcription, NusE participates in translation as part of the 30S ribosomal subunit (16–18).

A termination-resistant TEC also assembles during transcription of *rrn* operons in *E. coli* and other bacteria (19,20). In addition to Nus factors, ribosomal proteins S4, S2, L4 and L13 participate in transcription regulation (21,22). *BoxA* is highly conserved in all seven *E. coli rrn* operons. A promoter-proximal *BoxB*-like element is present but is not required for *rrn* antitermination (23). As is the case with λ, formation of the ternary NusB:NusE:*BoxA* complex is a key step during *rrn* processive antitermination (13).

The structure of the NusB:NusE$^{\Delta loop}$ complex, in which the 22 residue ribosome-binding loop of NusE was deleted, has recently been determined (24). Analysis of this structure and other data (25) suggest that NusE is the active partner of the complex and that NusB mainly acts as a loading factor for NusE, a notion that is

*To whom correspondence should be addressed. Tel: +49 921 55 3540; Fax: +49 921 55 3544; Email: roesch@unibt.de

© The Author(s) 2009. Published by Oxford University Press.
This is an Open Access article distributed under the terms of the Creative Commons Attribution Non-Commercial License (http://creativecommons.org/licenses/by-nc/2.5/uk/) which permits unrestricted non-commercial use, distribution, and reproduction in any medium, provided the original work is properly cited.

supported by the fact that NusE in a NusB deletion background could still support N antitermination and Nun termination (24). Although UV-crosslinking studies indicate that both NusB and NusE$^{\Delta loop}$ contact *BoxA* RNA, detailed structural information about the RNA binding of NusB and the ternary NusB:NusE:RNA complex is not currently available.

Several *nutR BoxA* mutants abolish N-mediated antitermination or Nun-mediated transcription arrest *in vivo* and/or *in vitro*, namely *nutR BoxA5* (G35U) (26), *nutR BoxA16* (C38A) (27), *nutR BoxA* (U39G) (28). Oddly, the 9-bp transversion mutant *nutR BoxA69* has little effect on N-mediated antitermination except to make it NusB-independent, and it was proposed that NusB competed for *BoxA* binding with an as yet unidentified inhibitor of N activity (14).

NusB101 (D118N) presents an intriguing gain of function variant that suppresses a block in N-mediated antitermination by NusA1 (L183R) and NusE71 (A86D) at 42°C (29,30). NusB^{D118N} has enhanced affinity for *rrn* and λ *nut BoxA* (29); for example, NusB^{D118N}:NusE can be UV-crosslinked to *BoxA*-containing RNAs more efficiently than wt NusB:NusE (24). However, whether the increased affinity originates from a charge effect, from different direct contacts of the amino acid at position 118 to the RNA, or from a combination of effects is not clear.

In the present study, we used biophysical and genetic approaches to delineate identity elements of *nut* RNA that are recognized by NusB and by heterodimeric NusB:NusE complex. Furthermore, we studied NusB D118 mutants to clarify the role of this amino acid in NusB:RNA and NusB:NusE:RNA interactions.

MATERIALS AND METHODS

Cloning, expression and protein purification of Nus-factors

The *nusB* gene was cloned *via* BamH1 and Nde1 restriction sites into the *E. coli* expression vector pET29b (Novagen, Madison, WI, USA). *Escherichia coli* strain BL21(DE3) (Novagen, Madison, WI, USA) harboring the recombinant plasmid was grown at 37°C in LB (Luria–Bertani) medium containing kanamycin (30 μg/ml) until an $OD_{600} = 0.5$ was reached, then the temperature was reduced to 20°C for 30 min and the cells were induced by 1 mM isopropyl 1-thio-β-D-galactopyranoside (IPTG). Cells were harvested 4 h after induction, resuspended in four times the pellet weight of lysis buffer (50 mM Tris, 150 mM NaCl, 1 mM DTT, pH 7.5), and lysed by using a micro-fluidizer (Microfluidics, Newton, MA, USA). After centrifugation the supernatant was dialyzed for 4 h against lysis buffer without NaCl and afterwards applied to a HeparinFF column (GE Healthcare, Munich, Germany) using a step gradient with increasing NaCl concentrations (0–1 M). For further purification the eluted fractions containing NusB were pooled and concentrated with Vivaspin concentrators (Vivascience, MWCO 5000 Da). The concentrated sample was applied to an S75 gel filtration column (GE Healthcare). The fractions containing NusB were pooled and dialyzed against buffer as used for fluorescence measurements (25 mM HEPES, 100 mM potassium acetate, pH 7.5). The identity and structural integrity of the purified protein was analyzed by 19% SDS–PAGE and NMR spectroscopy.

NusB mutations

For NusB^{D118N} (NusB101), NusB^{D118R}, NusB^{D118A}, NusB^{D118E} and NusB^{D118K} the mutation primers shown in Supplementary Table S1 were used. Mutations were introduced by using the QuikChange protocol (Stratagene, La Jolla, CA, USA). Expression and purification was as described for wildtype NusB. NusB^{K2E} was inherent in the original NusB pETM11-plasmid (24).

NusE:NusB complex

NusE was cloned *via* BamH1 and EcoR1 restriction sites into the *E. coli* expression vector pGEX-6P (GE Healthcare) (24). The recombinant plasmid encoded a GST-NusE fusion protein with an internal PreScission cleavage site following the GST-tag. *Escherichia coli* strain BL21(DE3) (Novagen) harboring the recombinant plasmid was grown at 37°C in LB medium containing ampicillin (100 μg/ml) until an $OD_{600} = 0.5$ was reached, then the temperature was reduced to 20°C for 30 min and the cells were induced by 1 mM IPTG. After induction overnight, the cells were harvested and resuspended in four times the pellet weight of lysis buffer (50 mM Tris, 150 mM NaCl, 1 mM DTT, pH 7.5). At this point, the NusB cell extract solved in the same buffer was added. After mixing for 20 min the cells were lysed with a micro-fluidizer (Microfluidics, Newton, MA, USA), and additional mixing was performed for 1 h to ensure correct formation of the NusB:NusE dimer. After centrifugation the dimer was purified from the supernatant *via* a GSTrap-FF column (GE Healthcare) using a one step elution (lysis buffer with 15 mM reduced gluthathione). The GST-NusE fusion protein was cleaved by PreScission protease while dialyzing against lysis buffer at 4°C overnight. The cleaved protein was reapplied to a GSTrap-FF column using the same step elution procedure, but this time collecting the flow-through. For further purification the eluted fractions containing NusB:NusE were pooled and concentrated with Vivaspin concentrators (Vivascience, MWCO 5000 Da). The concentrated sample was applied to an S75 gel filtration column (GE Healthcare). The fractions containing NusB:NusE were pooled and dialyzed against buffer as used for fluorescence measurements (25 mM HEPES, 100 mM potassium acetate, pH 7.5). The identity and structural integrity of the purified protein complexes were analyzed by 19% SDS–PAGE.

NusB^{D118E}–NusE$^{\Delta loop}$ production and purification for crystallization

Cloning of the genes encoding NusB and NusE$^{\Delta loop}$ has been described (24). Mutations were introduced by using the QuikChange protocol (Stratagene, La Jolla, CA, USA). To produce protein for crystallographic analysis, plasmids containing the genes of interest were

co-transformed into *E. coli* strain BL21(DE3) by electroporation. The cells were grown in auto-inducing medium (31) in the presence of the appropriate antibiotics to an OD_{600} of 0.5 at 37°C, and then incubated for an additional 16 h at 20°C. After harvesting at 4°C, the cell pellets were washed with binding buffer (50 mM Tris, pH 7.5, 150 mM NaCl) and stored at −80°C. Purification of the $NusB^{D118N}$:$NusE^{\Delta loop}$ complex followed a double affinity chromatography procedure as described for the NusB:$NusE^{\Delta loop}$ complex (24).

Crystallographic analysis

$NusB^{D118N}$:$NusE^{\Delta loop}$ complex (NusB101:$NusE^{\Delta loop}$; 16 mg/ml) was crystallized at 20°C *via* the sitting drop vapor diffusion method by mixing 1 ml of sample with 1 ml of reservoir solution (0.2 M potassium citrate, 20% PEG 3350). Crystals could be flash frozen in liquid nitrogen after transfer into 60% reservoir plus 40% glycerol. Diffraction data were collected at 100 K on beamline PXII (SLS, Villigen, Switzerland) using a MarCCD 225 mm detector. The data were processed with the XDS package (32).

The structure of the $NusB^{D118N}$:$NusE^{\Delta loop}$ complex was solved by molecular replacement using the coordinates of the NusB:$NusE^{\Delta loop}$ complex [PDB ID 3D3B; (24)]. The model was manually rebuilt using COOT (33) and refined by standard methodology using Refmac5 including TLS refinement (34). Each protein molecule in the crystallographic asymmetric unit represented a separate TLS group.

In vivo assays

nusB::Cam nusA^{+} or *nusB::Cam nusA1* mutants carrying λ*cI857* prophage were constructed. Wild-type and mutant NusB were supplied from a pBAD30 plasmid. Phage burst size after thermal induction was determined according to standard protocols.

Fluorescence equilibrium measurements

Various RNA sequences corresponding to the *nut* regions of the λ genome or to the *rrnG BoxA* of the *E. coli* genome (Supplementary Table S2) were used. Fluorescence equilibrium titrations were performed using an L-format Jobin–Yvon Horiba Fluoromax fluorimeter (Edison, NJ, USA). Extrinsic fluorescence measurements with 3′-6-carboxy-fluorescein (6-FAM)-labeled RNA were performed in fluorescence buffer as above in a total volume of 1 ml using a 10×4 mm quartz cuvette (Hellma, Müllheim, Germany). The excitation wavelength was 492 nm, and the emission intensity was measured at 516 nm applying a 500 nm cutoff filter. Anisotropic measurements were performed with slit widths of 4 nm and 3 nm for excitation and emission, respectively. All titration measurements were carried out at 25°C with 50 nM of 6-FAM-labeled RNA. Following sample equilibration, six data points with an integration time of 0.8 s were collected for each titration point.

Data fitting

Anisotropic data were fitted to a two-state binding model to determine the equilibrium dissociation constant (K_d) using standard software. The anisotropy was calculated from:

$$A = f_{complex} \cdot A_{complex} + f_{RNA} \cdot A_{RNA} \quad (1)$$

where A, $A_{complex}$, A_{RNA} are anisotropies and $f_{complex}$, f_{RNA} are fractional intensities. The change in fluorescence intensity has to be taken into account, so that the bound fraction is given by

$$\frac{[complex]}{[RNA]_0} = \frac{(A - A_{RNA})}{\left((A - A_{RNA}) + R \cdot \left(A_{complex} - A\right)\right)} \quad (2)$$

$$[complex] = \frac{\left(K_d + [P]_0 + [RNA]_0\right)}{\left(2[RNA]_0\right)} - \frac{\sqrt{\left(K_d + [P]_0 + [RNA]_0\right)^2 - 4[P]_0[RNA]_0}}{\left(2[RNA]_0\right)} \quad (3)$$

with A, anisotropy; A_{RNA}, initial free anisotropy; $A_{complex}$, anisotropy of the protein–RNA complex; P_0, RNA_0, total protein and RNA concentration, respectively; R, ratio of intensities of bound and free forms.

CD measurements

Far UV CD measurements were performed on a J-810 S spectropolarimeter with a CDF-426S temperature control unit (JASCO International, Tokyo, Japan). Samples were prepared by dialyzing protein solutions against 10 mM sodium phosphate buffer, pH 7.5. Spectra were recorded at 25°C in a wavelength range of 185–260 nm with 50 nm/min scanning speed in a 1 mm path length quartz cuvette (Hellma, Müllheim, Germany) at a protein concentration of 10 μM. Buffer spectra were subtracted and ten spectra were accumulated. In order to normalize the measured ellipticity the mean residue molar ellipticity was calculated as:

$$[\Theta]_{MRW} = \frac{\Theta}{(c \cdot d \cdot N)} \quad (4)$$

Θ, measured ellipticity; MRW, mean residue mass; c, protein concentration; d, path length; N, number of amino acids.

Thermal stability was analyzed by monitoring the CD signal at 222 nm during heating from 25°C to 90°C with a heating rate of 1°C/min. Quartz cuvettes with 1 cm path length equipped with a stirrer were used at a protein concentration of 2.5 μM. Both baselines and the transition region were fitted simultaneously:

$$y_{obs} = \frac{(y_n + m_n \cdot T_m)}{(1 + \exp(\Delta H_m / R(1/T_m - 1/T)))} + \frac{(y_d + m_d \cdot T) \cdot \exp(\Delta H_m / R \cdot (1/T_m - 1/T))}{(1 + \exp(\Delta H_m / R(1/T_m - 1/T)))} \quad (5)$$

y_{obs}, observed ellipticity; y_n, y_d y-intercepts of the baselines of native and denatured protein; m_n, m_d, baseline slopes.

ΔH_m is the enthalpy at the temperature of the melting point (T_M) (35,36). Evaluations were based on the assumption that the unfolding transition is a two-state reaction. The temperature dependence of ΔG_D (free energy of unfolding) can be predicted at any temperature from the modified Gibbs–Helmholtz equation:

$$\Delta G_D(T) = \Delta H_m(1 - T/T_m) - \Delta C_p((T_m - T) + T \cdot \ln(T/T_m)) \quad 6$$

Over the narrow temperature range of the transition effects of ΔC_P (change in heat capacity) are negligible. Therefore, the equilibrium constant of the unfolding reaction, K, is defined as

$$-R \cdot Tln(K) = \Delta H_m - T \cdot \Delta S_m = \Delta G_D \quad 7$$

$$K = \exp\left[\left(\frac{-\Delta H_m}{RT}\right) + \left(\frac{\Delta S_m}{R}\right)\right] \quad 8$$

where T is the temperature in Kelvin, R is the gas constant and ΔS_m is the entropy of unfolding at the melting point (T_M). When observing a two-state process with an experimental observable, y_{obs}, the equilibrium constant for the reaction is

$$K = \frac{(y_{obs} - (y_n + m_n \cdot T))}{((y_d + m_d \cdot T) - y_{obs})} \quad 9$$

By combining equations 7 and 9, ΔG_D can be calculated (36,37).

RESULTS

Fluorescence anisotropy measurements were performed to determine the dissociation constants of NusB or NusB :NusE and various RNA constructs (Tables 1 and 2).

Formation of the dimeric NusB:NusE complex enhances RNA binding affinity

NusB bound *rrnG BoxA-spacer* and *rrnG BoxA* with nearly identical efficiencies (dissociation constants K_d of 130 ± 20 nM and 200 ± 10 nM, respectively; Figure 1A, Table 1). The efficiency of NusB binding to λ *nutR BoxA-spacer*, *nutL BoxA-spacer* and *nutR BoxA* sequences was significantly lower (K_d values of ~1.5 μM; Figure 1B). The higher anisotropy of *nutR BoxA* relative to the other constructs reflects the different rotational correlation time relative to the large RNA constructs. Preformed NusB:NusE heterodimer bound to all RNAs tested with affinities more than an order of magnitude greater than NusB alone, consistent with the findings that both NusB and NusE in the NusB:NusE complex make RNA contacts (24). K_d values for the *rrnG BoxA-spacer* and the *rrnG BoxA* were 8 ± 2 and 5 ± 1 nM, respectively (Figure 1A; Table 2), and 90 ± 37 nM for *nutR BoxA-spacer*, 80 ± 22 nM for *nutL BoxA-spacer*, and 83 ± 8 nM for *nutR BoxA* (Figure 1C; Table 2). These data also indicate that contacts of NusE to the *spacer* region previously seen by UV-induced crosslinking (24) do not significantly increase the RNA affinity of the complex.

Protein RNA interaction takes place predominantly via BoxA

The binding of NusB and NusB:NusE to λ *nut BoxA-spacer* and *nutR BoxA* sequences with virtually identical affinities suggests that the spacer regions, shown previously to bind NusA (5), do not bind NusB or NusB:NusE. To confirm this, we measured binding to *spacer* alone. Specific binding of NusB or NusB:NusE to *nutL spacer* and *nutR spacer* was not observable in fluorescence titrations (Figure 1D). A slight increase of the fluorescence anisotropy signal with the NusB:NusE *nutR spacer* titration is consistent with unspecific binding with a K_d-value in the upper micromolar range.

BoxA mutations decrease binding affinity

Several *BoxA* mutations (Supplementary Table S2) affect λ N antitermination and HK022 Nun transcription arrest (14,26–28). We studied the effect of these mutations on NusB and NusB:NusE binding affinities. No interaction with the *boxA* transversion mutant *nutR BoxA69-spacer* and either NusB or NusB:E heterodimer was detected (Figure 2A and B; Tables 1 and 2), clearly indicating that the binding of these factors is *BoxA* RNA

Table 1. Dissociation constants for NusB monomer variants in nano molar

	NusB	$NusB^{D118N}$	$NusB^{D118A}$	$NusB^{D118E}$	$NusB^{D118K}$	$NusB^{D118R}$
rrnG BoxA-spacer	130 ± 20	24 ± 4	230 ± 140	370 ± 30	240 ± 40	500 ± 130
rrnG BoxA	200 ± 10	50 ± 15	1100 ± 100	150 ± 20	450 ± 50	800 ± 80
nutR BoxA-spacer	1200 ± 600	900 ± 300	nb	3200 ± 800	nb	nb
nutL BoxA-spacer	2200 ± 800	1400 ± 500				
nutR BoxA	1600 ± 100	290 ± 15	500 ± 140	1400 ± 100	600 ± 25	1000 ± 70
nutR-spacer	nb	nb				
nutL-spacer	nb	nb				
nutR BoxA5-spacer	3100 ± 1600	12 200 ± 1600				
nutR BoxA16-spacer	5100 ± 1400	6500 ± 2000				
nutR BoxA(U39G)-spacer	1600 ± 800	9000 ± 3400				
nutR BoxA69-spacer	nb	nb				

25 mM HEPES, 100 mM potassium acetate, pH 7.5.
nb = no binding detectable; empty cell = not determined. At least two independent experiments were performed per K_d. The relative molecular weights of the amino acids at residue 118 are A < N < D < E < K < R.

Table 2. Dissociation constants for NusB:NusE heterodimer variants in nano molar

	NusB:NusE	$NusB^{D118N}$: NusE	$NusB^{D118A}$: NusE	$NusB^{D118E}$: NusE	$NusB^{D118K}$: NusE	$NusB^{D118R}$: NusE	NusB: $NusE^{\Delta loop}$
rrnG BoxA-spacer	8 ± 2	24 ± 4	30 ± 5	125 ± 20	42 ± 6	26 ± 5	22 ± 2
rrnG BoxA	5 ± 1	25 ± 7	60 ± 5	135 ± 5	90 ± 4	65 ± 6	50 ± 5
nutR BoxA-spacer	90 ± 37	32 ± 11	700 ± 100	290 ± 90	110 ± 20	110 ± 28	360 ± 50
nutL BoxA-spacer	80 ± 22	40 ± 10					600 ± 60
nutR BoxA	83 ± 8	9 ± 1	60 ± 5	200 ± 20	75 ± 3	31 ± 2	160 ± 20
nutR Spacer	nb						
nutL Spacer	nb						
nutR BoxA5-spacer	5200 ± 1300						
nutR BoxA16-spacer	3400 ± 1800						
nutR BoxA(U39G)-spacer	1900 ± 700						
nutR BoxA69-spacer	nb						

25 mM HEPES, 100 mM potassium acetate, pH 7.5.
nb = no binding detectable; empty cell = not determined. At least two independent experiments were performed per K_d. The relative molecular weights of the amino acids at residue 118 are A < N < D < E < K < R.

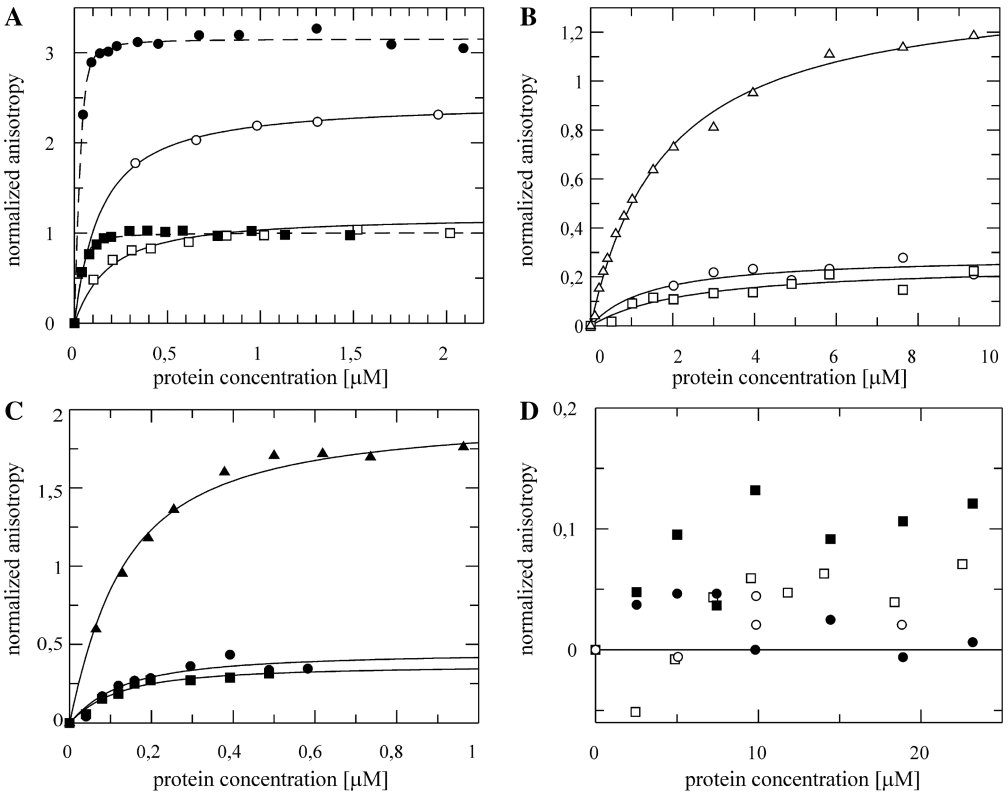

Figure 1. Fluorescence anisotropy titration of fluorescein labeled λ *nut* and *rrnG* RNAs with NusB (open markers) and NusB:NusE complex (filled markers). (**A**) A 50 nM *rrnG BoxA-spacer* (squares) and 50 nM *rrnG BoxA* (circles) titrated with NusB and NusB:NusE. (**B**) Fifty nanomolar *nutR BoxA-spacer* (circles), *nutL BoxA-spacer* (squares) and *nutR BoxA* (triangles) titrated with NusB. (**C**) A 50 nM *nutR BoxA-spacer* (circles), *nutL BoxA-spacer* (squares) and *nutR BoxA* (triangles) titrated with NusB/NusE. (**D**) A 50 nM *nutR spacer* (circles) and 50 nM *nutL spacer* (squares) titrated with NusB and NusB/NusE. Solid lines represent the best fit to equation (3).

sequence-dependent. This result supports the *in vivo* finding of Patterson *et al*. (14) that N antitermination on *BoxA69* fusions is NusB-independent. We next tested *BoxA* point mutants that inhibit N and Nun (Figure 2A and B; Tables 1 and 2). The *nutR BoxA5* mutation (G35U) reduced NusB binding 2- to 3-fold (K_d = 3.1 ± 1.6 μM). Interestingly, the affinity of NusB:NusE heterodimer for the mutant RNA was essentially identical to that of NusB (K_d = 5.2 ± 1.3 μM). NusB and NusB:NusE bound *nutR BoxA16* (C38A) with K_d values of 5.1 ± 1.4 μM and 3.4 ± 1.8 μM, respectively. The dissociation constants of NusB and NusB:NusE for *nutR BoxA* (U39G), which inhibits N, were 1.6 ± 0.8 μM and 1.9 ± 0.7 μM, respectively. Judged from their effects on the NusB and NusB:NusE binding affinities, G35 and C38 participate more tightly in protein binding than U39. The equivalent

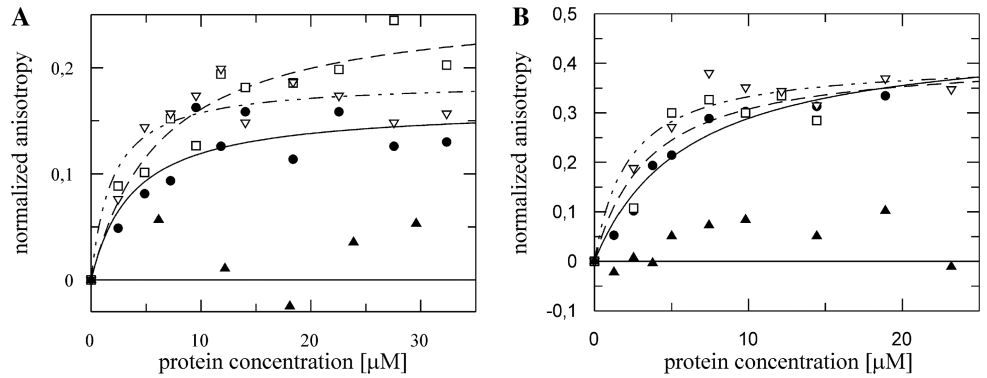

Figure 2. Fluorescence anisotropy, λ*nut BoxA* variants and NusB (**A**), NusB:NusE (**B**). Each titration was performed with 50 nM of fluorescein labeled RNA. *nutR BoxA5-spacer* (filled circle, fit: solid line), *nutR BoxA16-spacer* (open square, fit: dashed line), *nutR BoxA69-spacer* (filled triangle) and *nutR BoxA(U39G)-spacer* (open triangle, fit: dotted line). Lines represent the best fit to equation (3). For *nutR BoxA69-spacer* no interaction was observable, therefore no fitting was performed.

binding affinities of NusB and NusB:NusE heterodimer to these *BoxA* point mutants stands in sharp contrast to the enhanced binding of the heterodimer to wild-type *BoxA* sequences.

The NusB^{D118N} (NusB101) mutation affects RNA binding affinity

NusB^{D118N} is a gain- of-function mutation that enables NusB to override mutations in NusE and NusA that abrogate λ N-mediated antitermination (29,30). The dissociation constants for NusB^{D118N} complexes with *rrnG BoxA-spacer* and *rrnG BoxA* were 5- to 6-fold lower compared to wild-type NusB (Figure 3A; Table 3). Only small reductions in K_d were observed for the *nutL BoxA-spacer* and *nutR BoxA-spacer* complexes, whereas the dissociation constant for the complex of NusB^{D118N} with *nutR BoxA* decreased significantly from ~1600 nM to ~290 nM (Figure 3B; Table 1). In contrast, the mutation increased the K_d values about 3-fold for heterodimer complexes with *rrnG BoxA-spacer* and *rrnG BoxA* (Figure 3C, Table 2). NusB^{D118N}:NusE complexes with *nutR BoxA-spacer* and *nutL BoxA-spacer* sequences displayed 3- and 5-fold, respectively, lower K_d values for the mutant relative to the wild-type heterodimer (Figure 3D, Table 3). For the NusB^{D118N}:NusE complex with *nutR BoxA*, the K_d decreased by nearly an order of magnitude to 9 ± 1 nM (Figure 3D; Table 2). Thus, NusE did not further enhance the binding of NusB^{D118N} to *rrnG BoxA* or *rrnG BoxA-spacer*. However, NusE strongly stimulated the binding of NusB^{D118N} to sequences derived from *nutL* and *nutR*.

The structure of NusB^{D118N}:NusE$^{\Delta loop}$ closely resembles the structure of NusB:NusE$^{\Delta loop}$

NusE$^{\Delta loop}$ is a derivative of NusE that binds NusB and retains transcriptional but not translational activity (24). The NusB:NusE$^{\Delta loop}$ complex binds RNA that includes a *BoxA* sequence, although with lower efficiency than NusB:NusE [(24); Figure S1; Table 2]. Previous studies demonstrated that NusB^{D118N}:NusE$^{\Delta loop}$ bound RNA more tightly than NusB:NusE$^{\Delta loop}$. To ask if the increased RNA affinity of the NusB^{D118N}:NusE$^{\Delta loop}$ complex correlated with structural rearrangements compared to the NusB:NusE$^{\Delta loop}$ complex, we solved the crystal structure of the NusB^{D118N}:NusE$^{\Delta loop}$ complex by molecular replacement at 2.5 Å resolution (Figure 4). The structure was refined to R_{work} and R_{free} factors of 20.4% and 25.6%, respectively (Table 4). An asymmetric unit of the crystal contained three molecules each of NusB^{D118N} and NusE$^{\Delta loop}$, which formed three NusB^{D118N}:NusE$^{\Delta loop}$ complexes. Two of these complexes exhibited well-defined electron density, but the electron density map of the third complex was fragmentary: In that complex, residues 60–77 and 127–139 of NusB^{D118N} and residues 45–47 and 60–72 of NusE$^{\Delta loop}$ could not be unambiguously traced. The following discussion therefore refers to the structures of the two well defined complexes, which closely resemble each other [RMSD of 0.75 Å for 220 Cα atoms; calculated with SSM (38)].

The global structure of NusB^{D118N} in complex with NusE$^{\Delta loop}$ is very similar to that of wild-type NusB in isolation [PDB ID 1EY1; (39); rmsd of 2.54 Å for 110 Cα atoms; Figure 4]. Furthermore, the structure of the NusB^{D118N}:NusE$^{\Delta loop}$ complex is virtually identical to that of the NusB:NusE$^{\Delta loop}$ complex (RMSD of 0.85 Å for 220 Cα atoms; Figure 4B), demonstrating that the D118N mutation has no global conformational consequences. In particular, the positions and conformations of NusB residue N118 in the mutant and of residue D118 in the parent complex are essentially identical. Irrespective of the amino acid at position 118, the neighboring region undergoes identical adjustments upon NusE$^{\Delta loop}$ binding, during which the Cα position of residue 118 is repositioned by 2.8 Å (Figure 4C, inset). However, the D118N exchange induces a significant difference in the local electrostatic surface properties of the complex (Figure 4D). This observation is consistent with the idea that the increased RNA affinity of NusB^{D118N} or its complex with NusE$^{\Delta loop}$ is at least in part due to the replacement of a negatively charged residue with an uncharged residue at the RNA binding site, thus reducing repulsion with the negatively charged

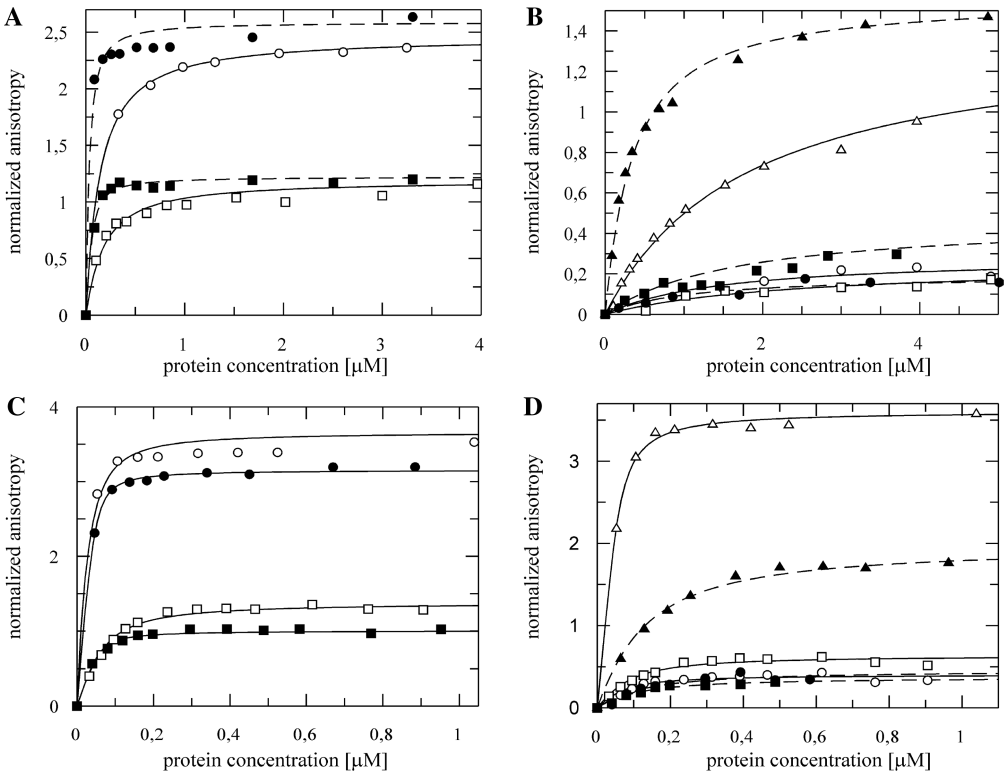

Figure 3. Fluorescence anisotropy measurements with fluorescein-labeled λ*nut* and *rrnG* RNAs towards $NusB^{D118N}$ (**A** and **B**) and $NusB^{D118N}$:NusE complex (**C** and **D**) (filled markers) compared to the wild-type NusB and NusB:NusE complex (open markers, data as in Figure 1A and C). (A) Fifty nanomolar *rrnG BoxA-spacer* (squares) and 50 nM *rrnG BoxA* (circles) titrated with $NusB^{D118N}$ and NusB; (B) 50 nM *nutR BoxA-spacer* (circles), *nutL BoxA-spacer* (squares) and *nutR BoxA* alone (triangles) titrated with Nus^{D118N} and NusB. (C) A 50 nM *rrnG BoxA-spacer* (squares) and 50 nM *rrnG BoxA* (circles) titrated $NusB^{D118N}$:NusE and NusB:NusE; (D) 50 nM *nutR BoxA-spacer* (circles), *nutL BoxA-spacer* (squares) and *nutR BoxA* (triangles) titrated with $NusB^{D118N}$:NusE and NusB:NusE. Dashed lines represent the best fit to equation (3) for $NusB^{D118N}$ and $NusB^{D118N}$/NusE, respectively. Solid lines the similar fit for wild-type NusB and NusB:NusE.

Table 3. Melting temperatures (T_M), free reaction enthalpy at the melting point ($\Delta H_{M,D}$) and Gibbs free energy of the unfolding reaction at 328K (ΔG_D) values for NusB variants (10 mM potassium phosphate, pH 7.5)

	T_M (K)	$\Delta H_{M,D}[T_M]$ (kJ/mol)	ΔG_D [328K] (kJ/mol)
NusB	337.8 ± 0.1	280 ± 4	8.3 ± 0.2
$NusB^{D118N}$	333.6 ± 0.1	174 ± 3	2.7 ± 0.2
$NusB^{D118A}$	333.5 ± 0.1	340 ± 4	5.6 ± 0.2
$NusB^{D118R}$	331.0 ± 0.1	298 ± 4	2.4 ± 0.2
$NusB^{D118E}$	334.5 ± 0.1	263 ± 3	5.8 ± 0.2
$NusB^{D118K}$	330.8 ± 0.1	244 ± 3	1.6 ± 0.2

sugar-phosphate backbone of the RNA. Alternatively, or in addition, introduction of an asparagine for an aspartate at position 118 may result in additional hydrogen bonds to the RNA.

The overall structures of various NusB118 mutants are highly similar

To investigate further the effect of amino acid variations at position 118, several point mutations with positively charged, negatively charged, and apolar amino acids were examined. All NusB variants show CD-spectra typical of α-helices, i.e. minima at 208 nm and 222 nm as well as a maximum at 190 nm (Figure 5A), with only minor differences from the wild-type protein spectrum. The melting temperatures of NusB and NusB D118 variants were determined by thermal unfolding. The CD signal at 222 nm, which we used to indicate melting, was reduced by all mutations, particularly by substitutions with positively charged residues. The Gibbs free energy of the unfolded species (ΔG_D) at 328 K thus ranges from 8.3 ± 0.2 kJ/mol for wild-type NusB to 1.6 ± 0.2 kJ/mol for $NusB^{D118K}$. The NusB variants, with the notable exception of $NusB^{D118N}$, show very similar unfolding transitions. The broader transition of $NusB^{D118N}$ indicates a lower value for the Gibbs free energy of the unfolding reaction at 328 K and for the free reaction enthalpy at the melting point [(35,36); Figure 5 and Table 3]. These relatively small differences indicate that the D118 point mutations do not lead to global NusB misfolding or to unstable NusB proteins.

Effects of other NusB D118 mutations on RNA binding

The binding properties of different NusB mutants dependent on the RNA were tested. Thus the binding of $NusB^{D118A}$ to *rrnG BoxA-spacer* was approximately as tight as $NusB^{+}$, whereas the affinity of the mutant for *rrnG BoxA* was 20% that of $NusB^{+}$ (Figure 6; Table 1). $NusB^{D118E}$ bound *rrnG BoxA* with wild-type efficiency but

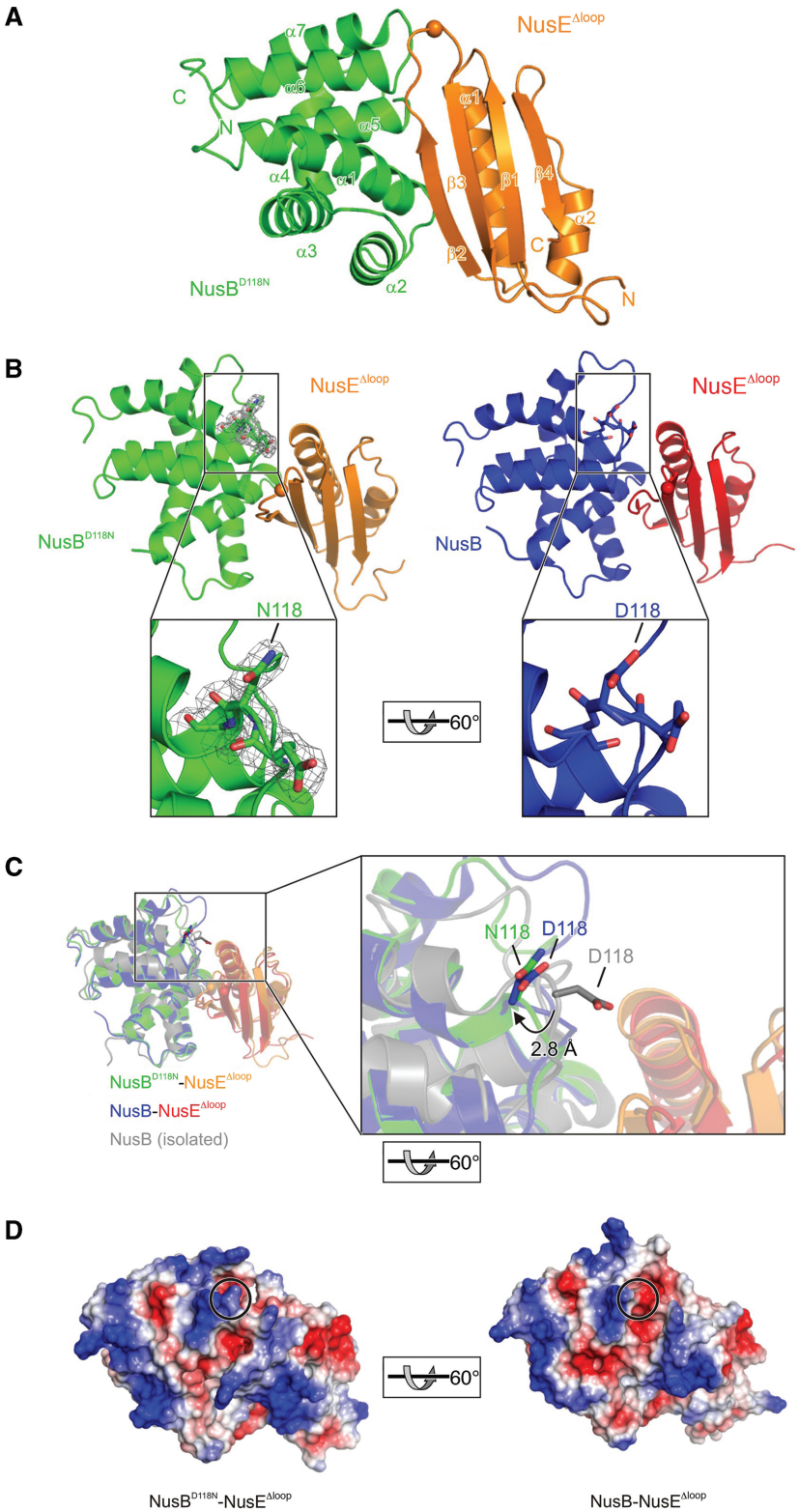

Figure 4. Structure of the NusB^{D118N}:NusE$^{\Delta loop}$ complex. (**A**) Ribbon plot of the *E. coli* NusB^{D118N}:NusE$^{\Delta loop}$ complex. NusB^{D118N}, green; NusE$^{\Delta loop}$, orange. Secondary structure elements and termini are labeled. The orange sphere marks the site at which the ribosome-binding loop of NusE has been replaced by a single serine. (**B**) Comparison of the NusB^{D118N}:NusE$^{\Delta loop}$ complex (left) with the NusB:NusE$^{\Delta loop}$ complex [right, PDB ID 3D3B; (24)]. Insets: closeup views of the residue 118 regions. The orientation relative to (A) is indicated. Gray mesh, final $2F_o - F_c$ electron density of the NusB^{D118N}:NusE$^{\Delta loop}$ structure contoured at the 1σ level and covering N118 and neighboring residues. The orientation relative to (A) is indicated. (**C**) Superimposition of the NusB:NusE$^{\Delta loop}$ complex [blue and red, PDB ID 3D3B; (24)] and of NusB [grey, PDB ID 1EY1; (39)] on the NusB^{D118N}:NusE$^{\Delta loop}$ complex (green and orange). Residues at position 118 are shown as sticks and a magnified view of the residue 118 region is provided (carbon, as the respective molecule; oxygen, red; nitrogen, blue). The orientation relative to (A) is indicated. (**D**) Comparison of the electrostatic surface potentials of the complexes. Blue, positive charge; red, negative charge. Left, NusB^{D118N}:NusE$^{\Delta loop}$ complex. Right, NusB:NusE$^{\Delta loop}$ complex. The positions of residue 118 are circled. The orientations are the same as in (B).

Table 4. Crystallographic data

	$NusB^{D118N} - NusE^{\Delta loop}$
Data collection	
Wavelength (Å)	0.9788
Temperature (K)	100
Space group	$I4_122$
Unit cell parameters (Å, °)	$a = 112.64$, $b = 112.64$, $c = 263.25$
Resolution (Å)	30.0–2.5 (2.6–2.5)[a]
Reflections	
Unique	29 761 (3263)
Completeness (%)	100 (100)
Redundancy	7.22 (7.42)
$I/\sigma(I)$	18.1 (4.1)
$R_{sym}(I)$[b]	8.6 (72.5)
Refinement	
Resolution (Å)	30.0–2.5 (2.56–2.50)
Reflections	
Number	29 753 (2178)
Completeness (%)	100 (100)
Test set (%)	5.0
R_{work}[c]	20.4 (23.1)
R_{free}[c]	25.6 (29.1)
Contents of AU[d]	
Protein molecules/refined atoms	3 $NusB^{Asp118Asn}$, 3 $NusE^{\Delta loop}$/5313
Water oxygen	155
Ions	1 K^+
Mean B-factors (Å^2)	
Wilson	52.7
Protein	60.5
Water	22.8
Ions	29.5
Ramachandran plot[e]	
Favored (%)	97.12
Allowed (%)	2.43
Outliers (%)	0.45
RMSD from target geometry	
Bond lengths (Å)	0.01
Bond angles (°)	1.22
RMSD B-factors (Å^2)	
Main chain bonds	0.41
Main chain angles	0.82
Side chain bonds	1.43
Side chain angles	2.48
PDB ID	3IMQ

[a]Data for the highest resolution shell in parentheses
[b]$R_{sym}(I) = \Sigma_{hkl}\Sigma_i|I_i(hkl) - \langle I(hkl)\rangle| / \Sigma_{hkl}\Sigma_i I_i(hkl)$; for n independent reflections and i observations of a given reflection; $\langle I(hkl)\rangle$ – average intensity of the i observations
[c]$R = \Sigma_{hkl}||F_{obs}| - |F_{calc}|| / \Sigma_{hkl}|F_{obs}|$; R_{work} – $hkl \notin$ T; R_{free} – $hkl \in$ T; T, test set.
[d]AU, asymmetric unit.
[e]Calculated with MolProbity (http://molprobity.biochem.duke.edu/) (40) RMSD, root-mean-square deviation.

associated with *rrnG BoxA-spacer* ~2-fold less well than $NusB^+$. We considered the possibility that replacing D118 with a positively charged residue might enhance binding through ionic interactions with the RNA ligand. This was not the case. Neither $NusB^{D118K}$ nor $NusB^{D118R}$ bound *rrnG* RNA with wild-type efficiency. The higher volumes of the lysine and arginine residues may induce unfavorable steric interactions, canceling out positive contributions to binding by electrostatic interactions with RNA. Consistent with this idea is our observation that $NusB^{D118R}$ bound *rrn* or *nutR BoxA* less efficiently than $NusB^{D118K}$, reflecting, perhaps, the larger volume of the former substitution. Of the various D118 substitutions, interaction with the *nutR BoxA-spacer* could be detected only for $NusB^{D118N}$ and $NusB^{D118E}$ (Figure 6 and Table 3). $NusB^{D118E}$ bound *nutR BoxA* as well as $NusB^+$. $NusB^{D118A}$ and $NusB^{D118K}$ bound *nutR BoxA* significantly better than wild-type NusB (Figure 6 and Tables 1 and 2).

NusE improves binding of NusB mutants

With the exception of $NusB^{D118E}$, NusE significantly enhanced mutant NusB binding to *rrnG* RNA, although no mutant except $NusB^{D118N}$ bound as well as $NusB^+$: NusE. NusE also enhanced binding to *nutR* sequences. Binding of NusB mutants to *nutR BoxA* was, except for $NusB^{D118E}$, at least as strong as $NusB^+$. Thus, NusE may foster additional RNA contacts, rendering NusB-mediated interactions less dominant (Figure 7 and Tables 1 and 2).

$NusB^{D118N}$, $NusB^{D118K}$ and $NusB^{D118R}$ suppress the *nusA1* ($nusA^{L183R}$) mutation *in vivo*

We next tested the NusB D118 mutants for suppression of *nusA1* ($nusA^{L183R}$). $nusA^{L183R}$ prevents phage λ growth at 42°C by blocking λ N antitermination. Over-expression of NusB D118 mutants in a $nusA^+$ λ *cI857* lysogen had modest negative effects on phage burst size (Table 5). The negatively charged $NusB^{D118E}$ was most inhibitory, reducing burst size to 32% of wild-type levels. In the $nusA^{L183R}$ background, all mutants except $NusB^{D118E}$ increased burst size >100-fold. $NusB^{D118N}$ suppressed $nusA^{L183R}$ with greatest efficiency, increasing burst size from <0.01% to 4.9% relative to $nusA^+$. $NusB^{D118K}$ and $NusB^{D118R}$ also significantly enhanced λ growth (to 2.2% and 3.3%, respectively, of *nusA+* titers). Suppression by $NusB^{D118A}$ was the least effective (0.5%). Taken together, these data suggest that replacing the negatively charged asp118 with an uncharged asparagine residue or a positively charged lysine or arginine residue significantly restores λ N activity in a $nusA^{L183R}$ strain. Poor suppression by the alanine substitution may reflect the lower molecular weight of this aminoacid relative to aspartate. Similarly, the inability of $NusB^{D118E}$ to restore λ growth may also be caused by steric effects due to the bulky glutamate side chain, in spite of its negative charge.

DISCUSSION

Processive transcription antitermination depends on formation of a multi-factorial ribonucleoprotein complex on the surface of RNAP in response to *nut* signaling sequences in the untranslated leader regions of transcripts. These factors include NusA, NusB, NusE and NusG (2–4). In the case of λ *nut*, λ N protein forms part of the complex, whereas the complex that forms at *rrn nut* includes the Nus proteins and a number of additional host factors (21,22). Protein–protein and protein–RNA interactions in these complexes are cooperative in the sense that a stable complex is assembled based on numerous, but often weak, binary interactions. While some

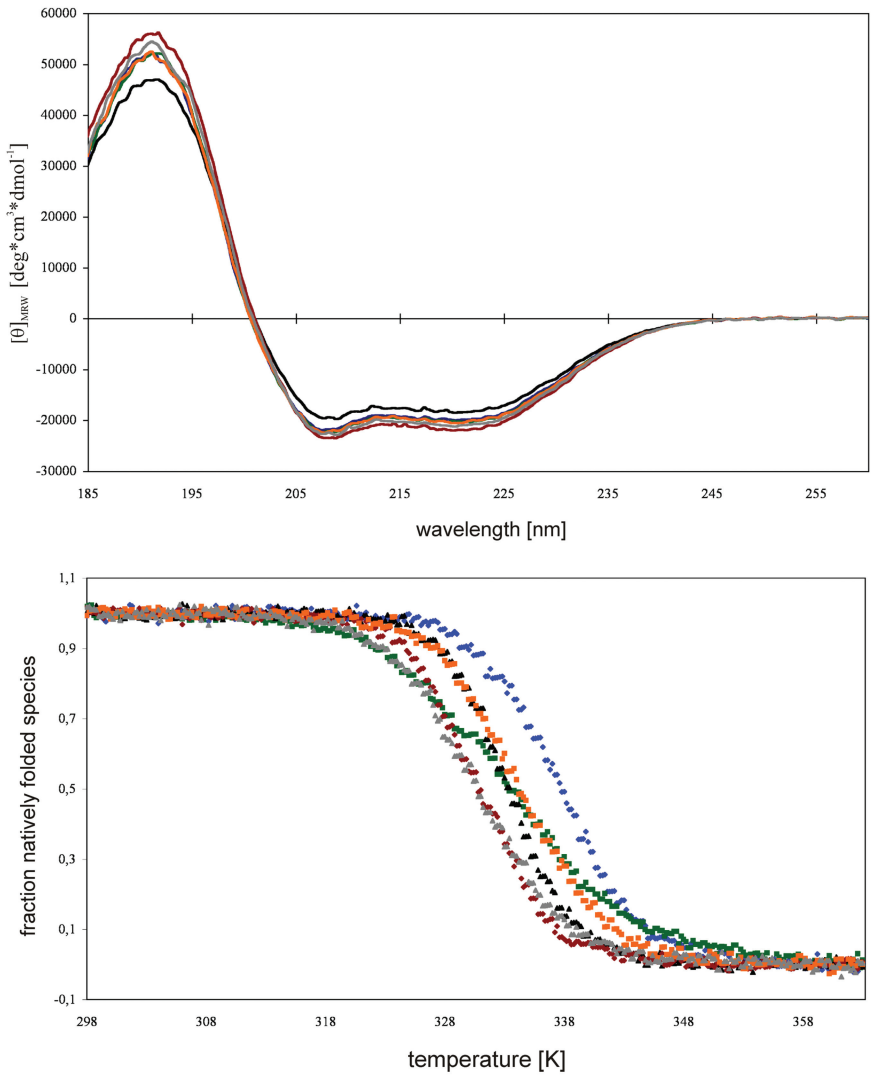

Figure 5. (**A**) Overlay of the CD-spectra for the NusB variants. Θ_{MRW} versus wavelength in nm. Θ_{MRW} was according to equation (4). (**B**) Thermal unfolding for the NusB variants. Fraction of the unfolded species versus absolute temperature. NusB (blue), NusB^{D118N} (green), NusB^{D118A} (black), NusB^{D118R}, (red), NusB^{D118E} (orange) and NusB^{D118K} (grey).

of these binary interactions have been mapped within the complexes, little is known about their relative strengths and how important these are for generating functional complexes. Here, we have used a combination of biophysical and functional studies to explore interactions between NusB or NusB:NusE complex and the *nut BoxA* RNA signaling sequence to which it binds.

We confirm that the affinity of NusB:NusE for *BoxA* is an order of magnitude higher than that of NusB alone (13), reflecting, presumably, the additional contacts that NusE makes with *BoxA*. We find that mutations in λ *nut BoxA* that inhibit λ N antitermination reduce NusB binding. However, in contrast to λ *nut BoxA*$^{+}$, the affinities of NusB and NusB:NusE for the mutant *BoxA* sequences are essentially identical. The mutations lie throughout *BoxA* and do not define the known sites of NusE–RNA interactions (24).

The K_d values reported above for the association of NusB or NusB:NusE with λ *nut BoxA* are similar to those reported by Greive and coworkers based on fluorescence anisotropy experiments (13). We note, however, a large difference with respect to *rrnG BoxA-spacer* binding. These authors report a K_d of 850 nM for NusB and 200 nM for NusB:NusE, whereas we observe values of 130 nM and 8 nM, respectively. Since the RNA sequences tested were identical, we suggest that the lower affinity seen by Greive *et al.* reflects the 5′ location of the fluorescent label on their RNA compared to the 3′ location used in our experiments. The N-terminus of NusB contacts both *rrn BoxA* and *nut BoxA* at their 5′-ends, and interference with these contacts by a 5′ label could increase the K_d values, although in an RNA sequence-dependent manner. Indeed, we find that the K2E mutation increased the K_d of the NusB *rrn BoxA-spacer* complex from 130 nM to 3600 nM, but raised the K_d of NusB binding to *nutL BoxA-spacer* only 2-fold (from 2200 nM to 5100 nM).

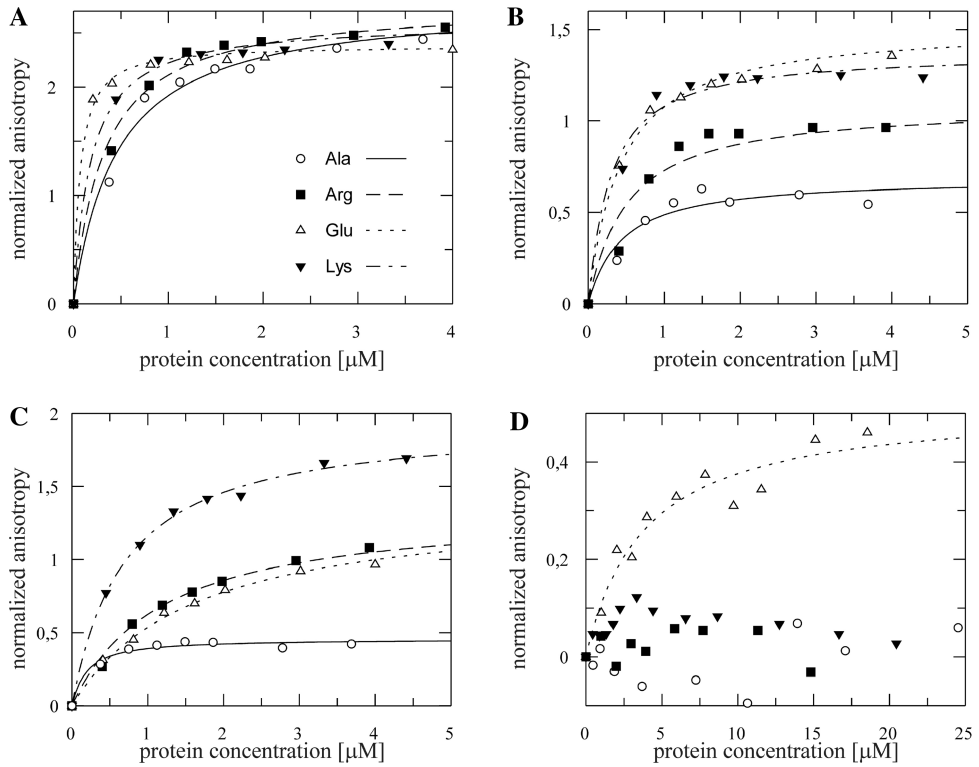

Figure 6. Fluorescence anisotropy measurements with fluorescein labeled λ*nut* or *rrnG* RNAs and NusB^{D118A} (open circle, fit: bold line), NusB^{D118R} (filled square, fit: dashed line), NusB^{D118E} (open triangle, fit: pointed line) and NusB^{D118K} (filled triangle, fit: dashed/pointed line). Lines represent the best fit to equation (3). (**A**) Fifty nanomolar *rrnG BoxA;* (**B**) 50 nM *rrnG BoxA-spacer;* (**C**) 50 nM *nutR BoxA*; and (**D**) 50 nM *nutR BoxA-spacer*.

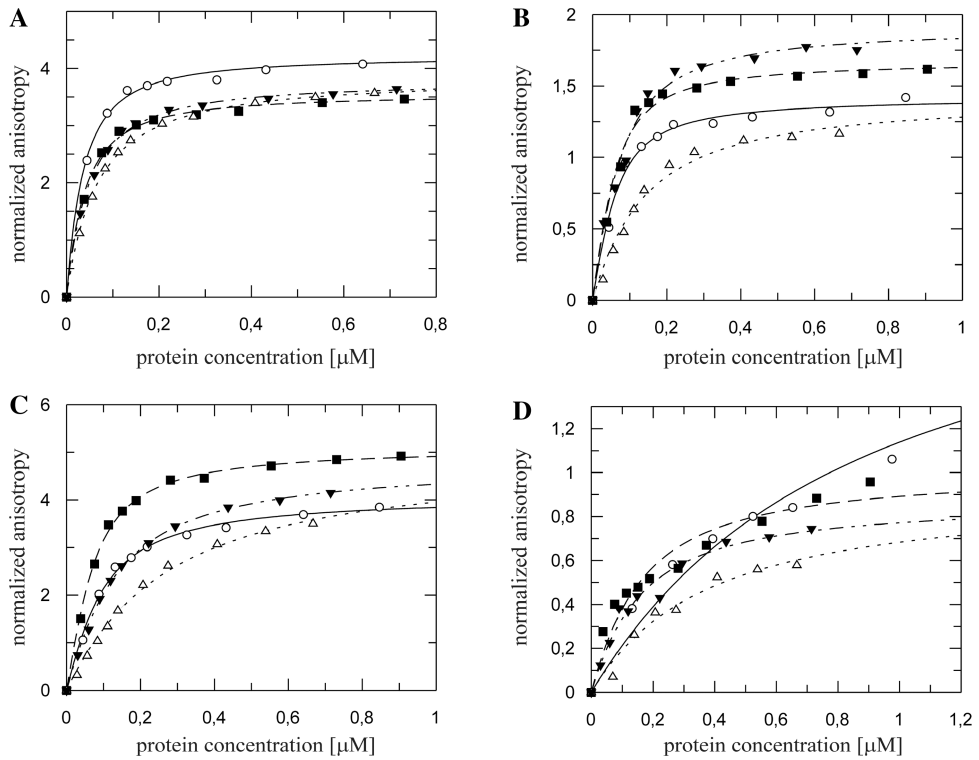

Figure 7. Fluorescence anisotropy measurements with fluorescein labeled λ*nut* and *rrnG* RNAs to NusB^{D118A}:NusE (open circle, fit: solid line), NusB^{D118R}:NusE (filled square, fit: dashed line), NusB^{D118E}:NusE (open triangle, fit: pointed line) and NusB^{D118K}:NusE (filled triangle, fit: dashed/pointed line). Lines represent the best fit to equation (3). (**A**) Fifty nanomolar *rrnG BoxA*; (**B**) 50 nM *rrnG BoxA-spacer*; (**C**) 50 nM *nutR BoxA*; and (**D**) 50 nM *nutR BoxA-spacer*.

Table 5. Strains are W3110 *nusB::Cam* λ*cI857* lysogens

nusB plasmid	*nusA*$^+$	*nusA1*	Suppression (%)
–	103	0.0004	<0.01
+	137	2	<0.01
D118N	85	4.2	4.9
D118A	74	0.4	0.5
D118E	44	0.005	<0.01
D118K	113	2.5	2.2
D118R	125	4.2	3.3

NusB is carried on pBAD30 and induced with 0.2% arabinose. Cells were grown overnight at 32°C in LB + ampicillin (50 μg/ml), diluted 1:100 into the same medium + 0.2% arabinose, and grown at 32°C for 1 h. λ was induced by temperature shift to 42°C for 90 min. Burst size was determined by plating the lysate on W3110 at 37°C. Cells were titered at 32°C prior to temperature shift; titers were equivalent for all strains. Values represent an average of two experiments; variation was <8 %.

We have also explored the phenotype of the NusB^{D118N} (NusB101) mutation. NusB^{D118N} suppresses mutations in NusA and NusE that inhibit λ N antitermination function (29,30). It has been proposed that an increase in the affinity of NusB^{D118N} for *nut* RNA compared to NusB$^+$ may compensate for weaker RNA (or protein) contacts of the mutant Nus proteins (24, 29). We show here that the D118N mutation enhances NusB binding to both *rrn BoxA* and λ *nut BoxA*. The mutation reduces binding to λ *nut BoxA* mutants, *BoxA5* and *BoxA(U39G),* but has no effect on binding to *BoxA16*. It will be interesting to test whether the D118N mutation further reduces λ N antitermination on *BoxA* mutant templates *in vivo*. D118N also enhances NusB binding to *nut BoxA* in complex with NusE. However, we find that the affinity of NusB^{D118N}:NusE for *rrn BoxA* is only 20% that of NusB$^+$:NusE. These data imply that D118N, although it optimizes the formation of the λ N antermination complex, interferes with the assembly of antitermination complexes on *rrn* operons.

The enhanced affinity of NusB^{D118N} to *BoxA* is not due to gross distortions in the shape of the NusE complex. Thus, the structure of NusB^{D118N}:NusE$^{\Delta loop}$ complex is virtually identical to NusB$^+$:NusE$^{\Delta loop}$, although the electrostatic surface properties are strongly affected (Figure 4D). In fact, CD spectroscopic analyses (Figure 5) show that NusB also structurally tolerates a number of other mutations at position 118. Thus, the effects of the D118 mutations on RNA binding are local.

D118 is located close to NusB residues that interact with *BoxA* RNA. It was suggested that removal of the negatively charged aspartate with the neutral asparagine residue might extend the NusB RNA-binding surface and that this might stabilize the antitermination complex and account for the suppression of *nusA1* and *nusE71*. Our results in general support this notion, although we find that the size of the D118 substitution also plays a role in the affinity of NusB for RNA.

The differential RNA affinities of the mutant NusB:NusE complexes roughly correlate with their *in vivo* suppression activity. We measured the burst sizes after induction of a λ *cI857* lysogen in *nusA*$^+$ and *nusA1* hosts. This assay, which reflects the ability of λ N to antiterminate, showed that the order of *nusA1* suppression efficiency was D118N > D118R > D118K > D118A. D118E failed to increase λ burst size over that seen for NusB$^+$. The binding affinities to *nut BoxA* for the mutants in complex with NusE was D118N > D118 > D118R > D118A > D118K > D118E. Note that the K_d of NusB$^+$ for *nut BoxA* (83 nM) was not significantly different from that of NusB^{D118K} (75 nM), yet the mutant NusB increased the λ burst size in a *nusA1* host at least 100-fold above the wild-type NusB level. This disjunction between RNA binding and N activation is, as yet, unexplained. It implies, however, that D118 may make functionally important contacts within NusB or with NusE.

We propose that D118 does not contact *BoxA*, but that removal of the negative charge permits such interaction. The location of position 118 opposite the NusB:NusE interaction surface renders an effect of mutations at this position on the NusB:NusE interaction unlikely. However, it cannot be ruled out completely, and a more definitive verdict needs further structural analysis of the NusB:NusE:*BoxA* complex. Study of how NusB mutations affect complex formation with NusE$^{\Delta loop}$ and alter its RNA binding properties might shed further light on the role of the NusE loop in RNA binding.

The results from our combined biophysical and genetic investigations illustrate how a particular protein–RNA interaction is fine-tuned with respect to other interactions within a functional ribonucleoprotein complex to achieve processive transcriptional antitermination. Furthermore, our results refine the mechanism by which NusB acts as a NusE RNA loading factor (24). NusB:NusE:RNA complex formation is entirely mediated by the *BoxA* sequences, whereas the *spacer* regions are necessary and sufficient for NusA binding (5). Sterically, simultaneous binding of these Nus factors to *nut* and *rrn* should be possible. There is, however, no evidence that NusA and NusB:NusE interact at *nut*, and no increase in *nut* binding by NusB:NusE was observed on NusA addition (15).

SUPPLEMENTARY DATA

Supplementary Data are available at NAR Online.

ACKNOWLEDGEMENTS

We would like to thank Ramona Heissmann for excellent technical assistance.

FUNDING

Deutsche Forschungsgemeinschaft (Ro617/16-1 to P.R.; Wa1126/3-1 to M.C.W.); National Institutes of Health (GM037219 to M.E.G.). Funding for open access charge: Universität Bayreuth.

Conflict of interest statement. None declared.

REFERENCES

1. Greenblatt,J., Nodwell,J.R. and Mason,S.W. (1993) Transcriptional antitermination. *Nature*, **364**, 401–406.
2. Das,A. (1993) Control of transcription termination by RNA-binding proteins. *Annu. Rev. Biochem.*, **62**, 893–930.
3. Borukhov,S., Lee,J. and Laptenko,O. (2005) Bacterial transcription elongation factors: New insights into molecular mechanism of action. *Mol. Microbiol.*, **55**, 1315–1324.
4. Roberts,J.W., Shankar,S. and Filter,J.J. (2008) RNA polymerase elongation factors. *Annu. Rev. Microbiol.*, **62**, 211–233.
5. Prasch,S., Jurk,M., Washburn,R.S., Gottesman,M.E., Wöhrl,B.M. and Rösch,P. (2009) RNA-binding specificity of *E. coli* NusA. *Nucleic Acids Res.*, **37**, 4736–4742.
6. Chattopadhyay,S., Garcia-Mena,J., DeVito,J., Wolska,K. and Das,A. (1995) Bipartite function of a small RNA hairpin in transcription antitermination in bacteriophage λ. *Proc. Natl Acad. Sci. USA*, **92**, 4061–4065.
7. Robert,J., Sloan,S.B., Weisberg,R.A., Gottesman,M.E., Robledo,R. and Harbrecht,D. (1987) The remarkable specificity of a new transcription termination factor suggests that the mechanisms of termination and antitermination are similar. *Cell*, **51**, 483–492.
8. Prasch,S., Schwarz,S., Eisenmann,A., Wöhrl,B.M., Schweimer,K. and Rösch,P. (2006) Interaction of the intrinsically unstructured phage λ N protein with *E. coli NusA*. *Biochemistry*, **45**, 4542–4549.
9. Bonin,I., Mühlberger,R., Bourenkov,G.P., Huber,R., Bacher,A., Richter,G. and Wahl,M.C. (2004) Structural basis for the interaction of *Escherichia coli* NusA with protein N of phage λ. *Proc. Natl Acad. Sci. USA*, **101**, 13762–13767.
10. Nodwell,J.R. and Greenblatt,J. (1993) Recognition of *boxA* antiterminator RNA by the *E.* coli antitermination factors NusB and ribosomal protein S10. *Cell*, **72**, 261–268.
11. Lüttgen,H., Robelek,R., Mühlberger,R., Diercks,T., Schuster,S.C., Kohler,P., Kessler,H., Bacher,A. and Richter,G. (2002) Transcriptional regulation by antitermination. Interaction of RNA with NusB protein and NusB/NusE protein complex of Escherichia coli. *J. Mol. Biol.*, **316**, 875–885.
12. Mason,S.W., Li,J. and Greenblatt,J. (1992) Host factor requirements for processive antitermination of transcription and suppression of pausing by the N protein of bacteriophage λ. *J. Biol. Chem.*, **267**, 19418–19426.
13. Greive,S.J., Lins,A.F. and von Hippel,P.H. (2005) Assembly of an RNA-protein complex. Binding of NusB and NusE (S10) proteins to *boxA* RNA nucleates the formation of the antitermination complex involved in controlling rRNA transcription in *Escherichia coli*. *J. Biol. Chem.*, **280**, 36397–36408.
14. Patterson,T.A., Zhang,Z., Baker,T., Johnson,L.L., Friedman,D.I. and Court,D.L. (1994) Bacteriophage lambda N-dependent transcription antitermination. Competition for an RNA site may regulate antitermination. *J. Mol. Biol.*, **236**, 217–228.
15. Mason,S.W. and Greenblatt,J. (1991) Assembly of transcription elongation complexes containing the N protein of phage λ and the *Escherichia coli* elongation factors NusA, NusB, NusG, and S10. *Genes Dev.*, **5**, 1504–1512.
16. Mizushima,S. and Nomura,M. (1970) Assembly mapping of 30S ribosomal proteins from *E. coli*. *Nature*, **226**, 1214.
17. Wimberly,B.T., Brodersen,D.E., Clemons,W.M.J., Morgan-Warren,R.J., Carter,A.P., Vonrhein,C., Hartsch,T. and Ramakrishnan,V. (2000) Structure of the 30S ribosomal subunit. *Nature*, **407**, 327–339.
18. Schluenzen,F., Tocilj,A., Zarivach,R., Harms,J., Gluehmann,M., Janell,D., Bashan,A., Bartels,H., Agmon,I., Franceschi,F. *et al.* (2000) Structure of functionally activated small ribosomal subunit at 3.3 Å resolution. *Cell*, **102**, 615–623.
19. Li,S.C., Squires,C.L. and Squires,C. (1984) Antitermination of *E. coli* rRNA transcription is caused by a control region segment containing lambda nut-like sequences. *Cell*, **38**, 851–860.
20. Quan,S., Zhang,N., French,S. and Squires,C.L. (2005) Transcriptional polarity in rRNA operons of *Escherichia coli nusA* and *nusB* mutant strains. *J. Bacteriol.*, **187**, 1632–1638.
21. Torres,M., Condon,C., Balada,J.M., Squires,C. and Squires,C.L. (2001) Ribosomal protein S4 is a transcription factor with properties remarkably similar to NusA, a protein involved in both non-ribosomal and ribosomal RNA antitermination. *EMBO J.*, **20**, 3811–3820.
22. Torres,M., Balada,J.M., Zellars,M., Squires,C. and Squires,C.L. (2004) *In vivo* effect of NusB and NusG on rRNA transcription antitermination. *J. Bacteriol.*, **186**, 1304–1310.
23. Berg,K.L., Squires,C. and Squires,C.L. (1989) Ribosomal RNA operon anti-termination. Function of leader and spacer region *box B-box A* sequences and their conservation in diverse micro-organisms. *J. Mol. Biol.*, **209**, 345–358.
24. Luo,X., Hsiao,H.H., Bubunenko,M., Weber,G., Court,D.L., Gottesman,M.E., Urlaub,H. and Wahl,M.C. (2008) Structural and functional analysis of the *E. coli* NusB-S10 transcription antitermination complex. *Mol. Cell*, **32**, 791–802.
25. DeVito,J. and Das,A. (1994) Control of transcription processivity in phage lambda: Nus factors strengthen the termination-resistant state of RNA polymerase induced by N antiterminator. *Proc. Natl Acad. Sci. USA*, **91**, 8660–8664.
26. Olson,E.R., Tomich,C.S. and Friedman,D.I. (1984) The *nusA* recognition site: Alteration in its sequence or position relative to upstream translation interferes with the action of the N antitermination function of phage lambda. *J. Mol. Biol.*, **180**, 1053–1063.
27. Robledo,R., Gottesman,M.E. and Weisberg,R.A. (1990) λ *nutR* mutations convert HK022 nun protein from a transcription termination factor to a suppressor of termination. *J. Mol. Biol.*, **212**, 635–643.
28. Baron,J. and Weisberg,R.A. (1992) Mutations of the phage lambda *nutL* region that prevent the action of nun, a site-specific transcription termination factor. *J. Bacteriol*, **174**, 1983–1989.
29. Court,D.L., Patterson,T.A., Baker,T., Costantino,N., Mao,X. and Friedman,D.I. (1995) Structural and functional analyses of the transcription-translation proteins NusB and NusE. *J. Bacteriol.*, **177**, 2589–2591.
30. Ward,D.F., DeLong,A. and Gottesman,M.E. (1983) *Escherichia coli nusB* mutations that suppress *nusA1* exhibit lambda N specificity. *J. Mol. Biol.*, **168**, 73–85.
31. Studier,F.W. (2005) Protein production by auto-induction in high density shaking cultures. *Protein Expr. Purif.*, **41**, 207–234.
32. Kabsch,W. (1993) Automatic processing of rotation diffraction data from crystals of initially unknown symmetry and cell constants. *J. Appl. Chrystallogr.*, **26**, 795–800.
33. Emsley,P. and Cowtan,K. (2004) Coot: Model-building tools for molecular graphics. *Acta Chrystallogr. D*, **60**, 2126–2132.
34. Winn,M.D., Musshudov,G.N. and Papiz,M.Z. (2003) Macromolecular TLS refinement in REFMAC at moderate resolutions. *Methods Enzymol.*, **374**, 300–321.
35. Santoro,M.M. and Bolen,D.W. (1988) Unfolding free energy changes determined by the linear extrapolation method. 1. Unfolding of phenylmethanesulfonyl α-chymotrypsin using different denaturants. *Biochemistry*, **27**, 8063–8068.
36. Swint,L. and Robertson,A.D. (1993) Thermodynamics of unfolding for turkey ovomucoid third domain: Thermal and chemical denaturation. *Protein Sci.*, **2**, 2037–2049.
37. Mayr,L.M., Landt,O., Hahn,U. and Schmid,F.X. (1993) Stability and folding kinetics of ribonuclease T1 are strongly altered by the replacement of cis-proline 39 with alanine. *J. Mol. Biol.*, **231**, 897–912.
38. Krissinel,E. and Henrick,K. (2004) Secondary-structure matching (SSM), a new tool for fast protein structure alignment in three dimensions. *Acta Chrystallogr. D*, **60**, 2256–2268.
39. Altieri,A.S., Mazzulla,M.J., Horita,D.A., Coats,R.H., Wingfield,P.T., Das,A., Court,D.L. and Byrd,R.A. (2000) The structure of the transcriptional antiterminator NusB from *Escherichia coli*. *Nat. Struct. Biol.*, **7**, 470–474.
40. Davis,I.W., Murray,L.W., Richardson,J.S. and Richardson,D.C. (2004) MOLPROBITY: Structure validation and all-atom contact analysis for nucleic acids and their complexes. *Nucleic Acids Res.*, **32**, W615–W619.